Supporting Information for

Isomeric Effects on the Acidity of Al_{13} Keggin Clusters in Porous Ionic Crystals

Wei Zhou,[a] Naoki Ogiwara,[a] Zhewei Weng,[a] Nanako Tamai,[a] Congcong Zhao,[b] Li-Kai Yan,[b] and Sayaka Uchida*[a]

[a]Department of Basic Science, School of Arts and Sciences, The University of Tokyo, Komaba, Meguro-ku, Tokyo 153-8902, Japan

[b]Institute of Functional Material Chemistry, Faculty of Chemistry, Northeast Normal University, Changchun 130024, P.R. China.

Table of contents

Title	Pages
Experimental Section	**S3–4**
Table S1. Pinacol to pinacolone rearrangement over various solid catalysts and conditions	**S5**
Table S2. Natural bond orbital (NBO) charges of oxygens in $[\delta\text{-}Al_{13}O_4(OH)_{24}(H_2O)_{12}]^{7+}$	**S6**
Table S3. Natural bond orbital (NBO) charges of oxygens in $[\varepsilon\text{-}Al_{13}O_4(OH)_{24}(H_2O)_{12}]^{7+}$	**S7**
Table S4. Natural bond orbital (NBO) charges of oxygens in $[\alpha\text{-}CoW_{12}O_{40}]^{6-}$	**S8**
Fig. S1 Powder XRD patterns of **δ-Al$_{13}$-CoW$_{12}$**.	**S9**
Fig. S2 Experimental (open circles) and calculated (red solid line) PXRD patterns of **δ-Al$_{13}$-CoW$_{12}$** by the Le Bail method.	**S9**
Fig. S3 Thermogravimetry of **δ-Al$_{13}$-CoW$_{12}$**.	**S10**
Fig. S4 IR spectra of **δ-Al$_{13}$-CoW$_{12}$**.	**S10**
Fig. S5 Calibration curves of (a) Na (λ = 589.0 nm) and (b) K (λ = 766.5 nm) in AAS.	**S11**
Fig. S6 Wide scan XPS spectra.	**S12**
Fig. S7 Solid state ^{27}Al-MASNMR spectra.	**S12**
Fig. S8 Solution ^{1}H-NMR spectrum (toluene-d_8) of the filtrate after the pinacol rearrangement catalyzed by **δ-Al$_{13}$-CoW$_{12}$**.	**S13**
Fig. S9 GC chart of the pinacol rearrangement catalyzed by **δ-Al$_{13}$-CoW$_{12}$**.	**S14**
Fig. S10 Time course of pinacol rearrangement catalyzed by **δ-Al$_{13}$-CoW$_{12}$**.	**S15**
Fig. S11 PXRD patterns of **δ-Al$_{13}$-CoW$_{12}$**. After reaction or evacuation at 373K.	**S15**
References	**S16**

Experiment Section

Synthesis. The solution containing $[\delta\text{-}Al_{13}O_4(OH)_{24}(H_2O)_{12}]^{7+}$ (**δ-Al$_{13}$**) was prepared according to a modification of the preparation of $[\varepsilon\text{-}Al_{13}O_4(OH)_{24}(H_2O)_{12}]^{7+}$ (**ε-Al$_{13}$**)[1] as described below. Into 200 mL of water, 12 g of $AlCl_3$ was added (0.45 mol L^{-1} $AlCl_3$(aq)) and stirred at 353 K (solution A). Into 450 mL of water, 4.5 g of NaOH was added (0.25 mol L^{-1} NaOH(aq)), and this solution was slowly added to solution A over 15 min under continuous stirring (pH 3.9). Then, the solution was kept at 368 K for another 2 days (pH 3.8) (denoted as **δ-Al$_{13}$** solution). $K_6[\alpha\text{-}CoW_{12}O_{40}]\cdot nH_2O$ was synthesized according to previous reports.[2,3] The ionic crystal (**δ-Al$_{13}$-CoW$_{12}$**) was synthesized as follows: 10 mL of 6.0 mmol L^{-1} aqueous solution of $K_6[\alpha\text{-}CoW_{12}O_{40}]\cdot nH_2O$ was added to 15 mL of **δ-Al$_{13}$** solution containing NaCl 150 mg (2.5 mmol), followed by immediate and spontaneous precipitation (solution B). Solution B was left under ambient conditions, and blue rod-shaped crystals were obtained through dissolution−recrystallization of the precipitate. The crystals were washed with distilled water three times (yield is 70% based on POM). The ionic crystal $[\varepsilon\text{-}Al_{13}O_4(OH)_{24}(H_2O)_{12}][\alpha\text{-}CoW_{12}O_{40}](OH)\cdot 41H_2O$ (**ε-Al$_{13}$-CoW$_{12}$**) was synthesized and characterized according to our previous work.[1]

Characterization. Inductively coupled plasma atomic emission spectroscopy (ICP-AES; Shimadzu, ICPE-9000) was used for the quantitative analysis of inorganic elements (Al, Co, W). Atomic absorption spectroscopy (AAS) analysis (Hitachi, ZA3000) was used for the quantitative analysis of alkali metals. See Fig. S2 for the calibration curves of Na (λ = 589.0 nm) and K (λ = 766.5 nm). Prior to the ICP-AES and AAS measurements, conc. HNO_3 (1 mL) was added to about 10 mg of the compounds (accurately weighed) to dissolve the solid completely into water (100 mL). According to the elemental analysis and thermogravimetry (Fig. S3), the chemical formula of **δ-Al$_{13}$-CoW$_{12}$** was determined as follows: $[\delta\text{-}Al_{13}O_4(OH)_{24}(H_2O)_{12}][\alpha\text{-}CoW_{12}O_{40}](OH)\cdot 22H_2O$. AAS (Na, K) and ion-exchange chromatography (Cl) showed that **δ-Al$_{13}$-CoW$_{12}$** does not contain Na, K, or Cl (see Fig. S5 and S6 for the details). Elemental analysis for **δ-Al$_{13}$-CoW$_{12}$** (calcd): Al 8.0 (7.85), Co 1.542(1.32), W 51.8 (49.4). X-ray photoelectron spectroscopy (XPS) was conducted with an PHI5000 VersaProbe (ULVAC-PHI inc.) equipped with an aluminum anode (Al K α = 1486.6 eV) operating at 25 W. IR spectra were measured by the KBr pellet method with a JASCO FT/IR 4100 spectrometer (JASCO) equipped with a TGS detector. Solid-state ^{27}Al and ^{1}H-MAS NMR spectra were measured with a Bruker AVANCE III 400 WB spectrometer (Bruker) equipped with a 4 mm standard probe operating at 400.18 MHz and a MAS rate of 14 kHz. Thermogravimetry was conducted with a Thermo Plus 2 thermogravimetric analyzer (Rigaku) with α-Al_2O_3 as a reference under a dry N_2 flow (100 mL min^{-1}) in the temperature range of 303−773 K. Powder XRD patterns were measured with a New ADVANCE D8 X-ray diffractometer (Bruker) by using Cu Kα radiation (λ = 1.54056 Å, 40 kV−40 mA) at 1.8 deg min^{-1}. **δ-Al$_{13}$-CoW$_{12}$** was dried in the oven at 373 K for 24 h to remove both the water of crystallization and aqua ligands of δ-Al_{13}, which is denoted as **δ-Al$_{13}$-CoW$_{12}$** (dried at 373 K). The sizes of the apertures of **δ-Al$_{13}$-CoW$_{12}$** and **ε-Al$_{13}$-CoW$_{12}$** were estimated by the void analysis tool of Mercury structure visualization software (CCDC).

Catalytic Reaction. Pinacol rearrangement was carried out in a glass reactor equipped with a magnetic stirrer. In a typical run, a mixture of pinacol (0.667 mmol), naphthalene (0.267

mmol, internal standard), and **δ-Al_{13}-CoW_{12}** (0.067 mmol) in toluene (2 mL) were stirred under air at 373 K. The reaction progress was followed by gas chromatography using a GC-2014 (Shimadzu) fitted with an InertCap 5 capillary column (GL Sciences) and a flame ionization detector.

Computation details. The density functional theory (DFT) calculations were performed using Gaussian 09 program package.[4] The geometric structures of $[\delta\text{-}Al_{13}O_4(OH)_{24}(H_2O)_{12}]^{7+}$, $[\varepsilon\text{-}Al_{13}O_4(OH)_{24}(H_2O)_{12}]^{7+}$ and $[\alpha\text{-}CoW_{12}O_{40}]^{6-}$ were optimized with B3LYP hybrid functional.[5] The LANL2DZ[6] was applied for Co and W atoms, and 6-31G(d)[7] was used to describe H, O, and Al atoms. The solvent effect was included with the conductor-like polarizable continuum model (CPCM)[8] and water solvent.

Table S1. Pinacol to pinacolone rearrangement over various solid catalysts and conditions

Catalyst	Temp [K]	Solvent	Time [h]	Conv. [%]	Selec.[a] [%]	Reference
H-ZSM-5	393	-	4	80	90	1
Ca-HY	393	-	4	70	88	1
La-HY	393	-	4	68	82	1
Nafion-H	448	-	0.6	92	75	2
Fe-AlPO	383	Toluene	3	69	81	3
Ni-AlPO	383	Toluene	3	50	80	3
Cu-AlPO	383	Toluene	3	54	80	3
Fe-ZSM-5	383	Toluene	6	0	-	4
Fe-MCM-41	383	Toluene	6	33	64	4
MCM-41	383	Toluene	6	13	14	4
Phosphonate-polysilsesquioxane	413	-	12	-	80[d]	5
Fe-Na-montmorillonite[b]	398	-	1	34	100	6
Al_{13}-montmorillonite[b]	398	-	1	100	100	6
Fe-Al_{13}-montmorillonite[b]	398	-	1	100	100	6
None	573−723	scH_2O	-	100	100	8
$H_4SiMo_{12}O_{40}$	423	-	1	100	44[c]	9
$H_3PMo_{12}O_{40}$	423	-	1	100	43[c]	9
$H_4SiW_{12}O_{40}$	423	-	1	100	71	9
$H_3PW_{12}O_{40}$	423	-	1	100	78	9
$[Cr_3O(OOCPh)_6(H_2O)]_4[SiW_{12}O_{40}]$	373	Toluene	12	100	79	10
$[Fe_3O(OOCPh)_6(H_2O)]_4[SiW_{12}O_{40}]$	373	Toluene	6	100	80	10
Al_2O_3	473	-	1	62	44	11
Aluminum phosphate	473	-	1	62	46	11
SiO_2	473	-	1	34	42	11
ZrO_2	473	-	1	31	44	11
POM6-*N*	373	Toluene	40	31	18	12
POM6-*P*	373	Toluene	40	76	54	12
Al13-sulfate	373	Toluene	40	4	2	12
$K_6CoW_{12}O_{40}$	373	Toluene	40	6	5	12
$[Al(Salphen)(H_2O)_2]_3[PW_{12}O_{40}]$	393	Toluene	24	86.9	66.6	13

a: by-product is 2,3-dimethyl-1,3-butadiene. b: catalyst : reactant = 5 : 1. c: by-product is acetone. (1) *J. Mol. Catal.* 1994, **87**, 39–46. (2) *Tetrahedron* 1994, **50**, 8195–8202. (3) *Microporous Mesoporous Mater*. 1998, **21**, 505–515. (4) *J. Mol. Catal. A: Chemical* 2002, *181*, 189−200. (5) *Chem. Commun.* 2001, 67–68. (6) *J. Chem. Soc. Faraday Trans.* 1997, **93**, 1591−1599. (7) *J. Am. Chem. Soc.* 2002, **124**, 5962–5963. (8) *J. Am. Chem. Soc.* 2000, **122**, 1908−1918. (9) *J. Mol. Catal. A: Chemical*. 1996, **107**, 305–311. (10) *Inorg. Chem.* 2012, **51**, 775−777. (11) *Indian J. Chem. Technol.* 2005, **12**, 447–454. (12) *Cryst. Growth Des*. 2016, **16,** 4968−4974 (13) *Dalton Trans*. 2017, **46**, 3105–3109.

Table S2 Natural bond orbital (NBO) charges of oxygens in $[\delta\text{-}Al_{13}O_4(OH)_{24}(H_2O)_{12}]^{7+}$ (Molecular structure viewed from the (a) frontside and (b) backside)

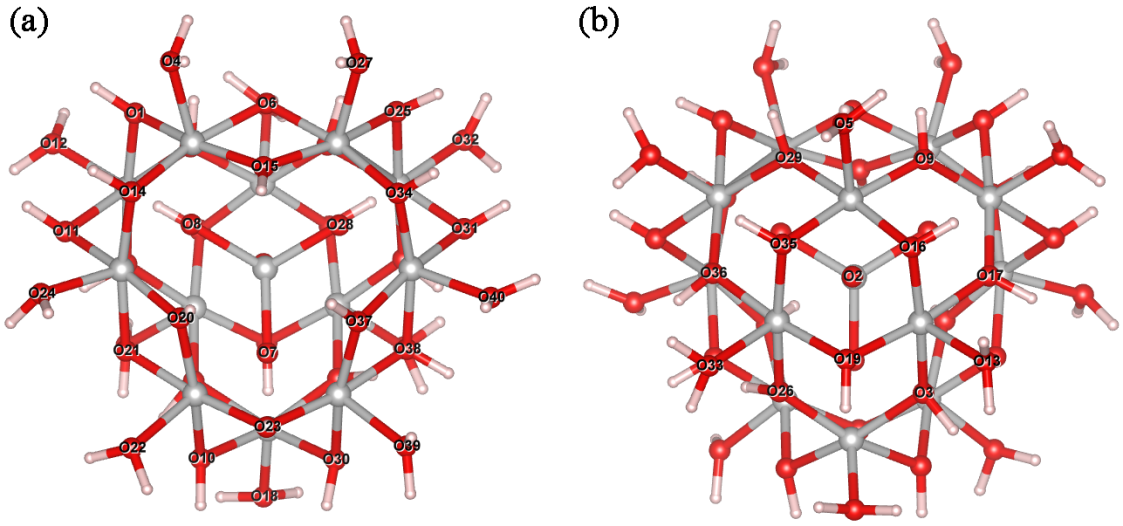

Atomic number	Charge	Atomic number	Charge
O1	–1.203	O21	–1.181
O2	–1.467	O22	–0.986
O3	–1.190	O23	–1.196
O4	–0.985	O24	–0.987
O5	–0.994	O25	–1.196
O6	–1.185	O26	–1.198
O7	–1.465	O27	–0.986
O8	–1.463	O28	–1.463
O9	–1.192	O29	–1.189
O10	–1.203	O30	–1.195
O11	–1.196	O31	–1.195
O12	–0.996	O32	–0.989
O13	–0.992	O33	–0.990
O14	–1.192	O34	–1.203
O15	–1.189	O35	–1.183
O16	–1.185	O36	–1.195
O17	–1.188	O37	–1.190
O18	–0.991	O38	–1.182
O19	–1.189	O39	–0.989
O20	–1.185	O40	–0.991

Table S3 Natural bond orbital (NBO) charges of oxygens in $[\varepsilon\text{-}Al_{13}O_4(OH)_{24}(H_2O)_{12}]^{7+}$ (Molecular structure viewed from the (a) frontside and (b) backside)

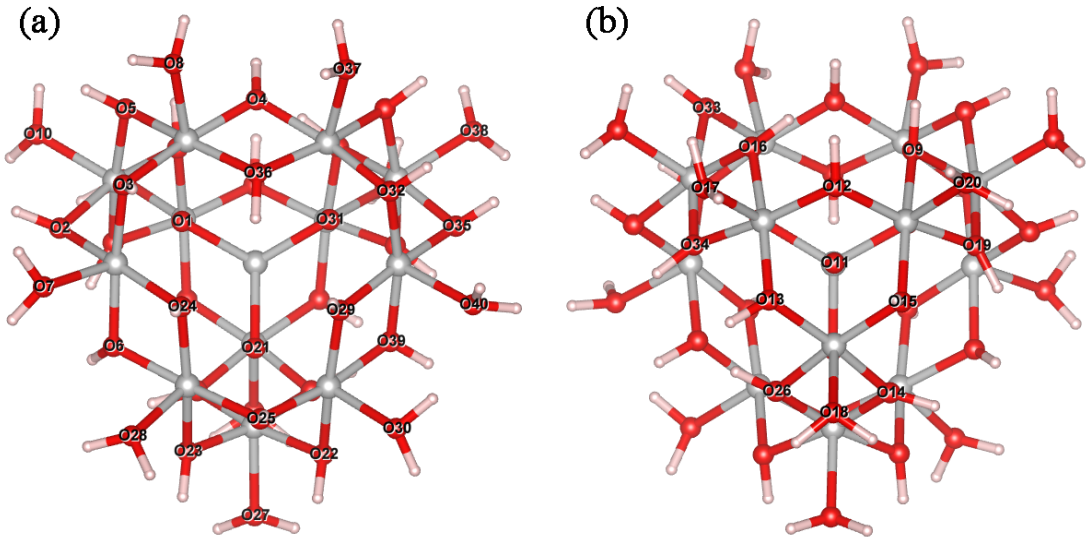

Atomic number	Charge	Atomic number	Charge
O1	−1.448	O21	−1.449
O2	−1.188	O22	−1.194
O3	−1.192	O23	−1.190
O4	−1.189	O24	−1.196
O5	−1.194	O25	−1.193
O6	−1.187	O26	−1.183
O7	−0.988	O27	−0.987
O8	−0.986	O28	−0.991
O9	−1.188	O29	−1.185
O10	−0.985	O30	−0.985
O11	−1.449	O31	−1.448
O12	−1.188	O32	−1.191
O13	−1.193	O33	−1.195
O14	−1.190	O34	−1.182
O15	−1.194	O35	−1.188
O16	−1.187	O36	−1.182
O17	−0.983	O37	−0.986
O18	−0.983	O38	−0.986
O19	−1.182	O39	−1.192
O20	−0.982	O40	−0.984

Table S4 Natural bond orbital (NBO) charges of oxygens in $[\alpha\text{-}CoW_{12}O_{40}]^{6-}$ (Molecular structure viewed from the (a) frontside and (b) backside)

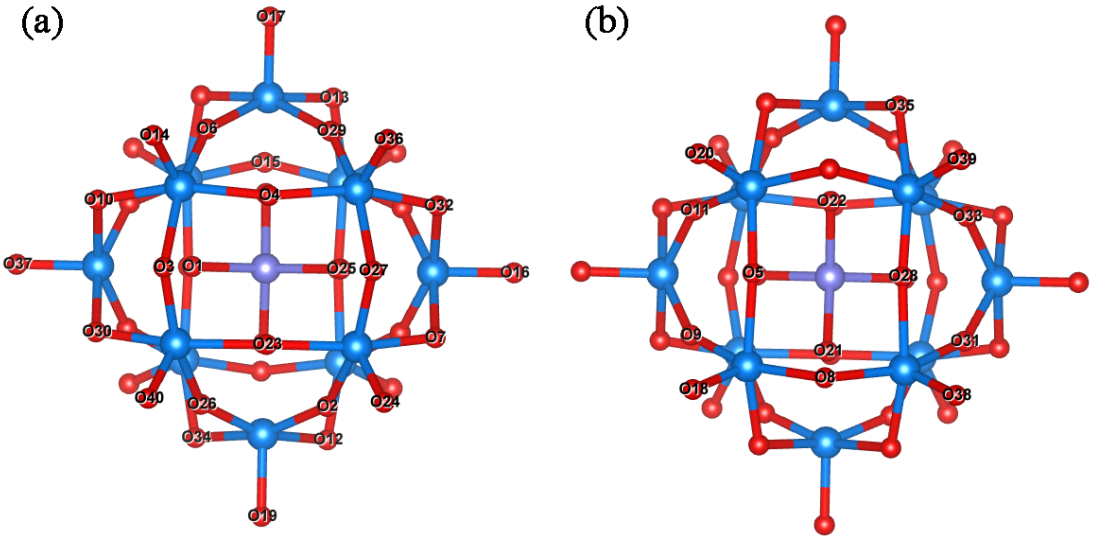

Atomic number	Charge	Atomic number	Charge
O1	–0.965	O21	–0.965
O2	–0.687	O22	–0.965
O3	–0.714	O23	–0.687
O4	–0.695	O24	–0.580
O5	–0.693	O25	–0.965
O6	–0.693	O26	–0.697
O7	–0.708	O27	–0.708
O8	–0.712	O28	–0.689
O9	–0.695	O29	–0.687
O10	–0.687	O30	–0.704
O11	–0.687	O31	–0.694
O12	–0.714	O32	–0.716
O13	–0.714	O33	–0.689
O14	–0.581	O34	–0.704
O15	–0.707	O35	–0.714
O16	–0.588	O36	–0.588
O17	–0.581	O37	–0.580
O18	–0.581	O38	–0.581
O19	–0.588	O39	–0.588
O20	–0.581	O40	–0.588

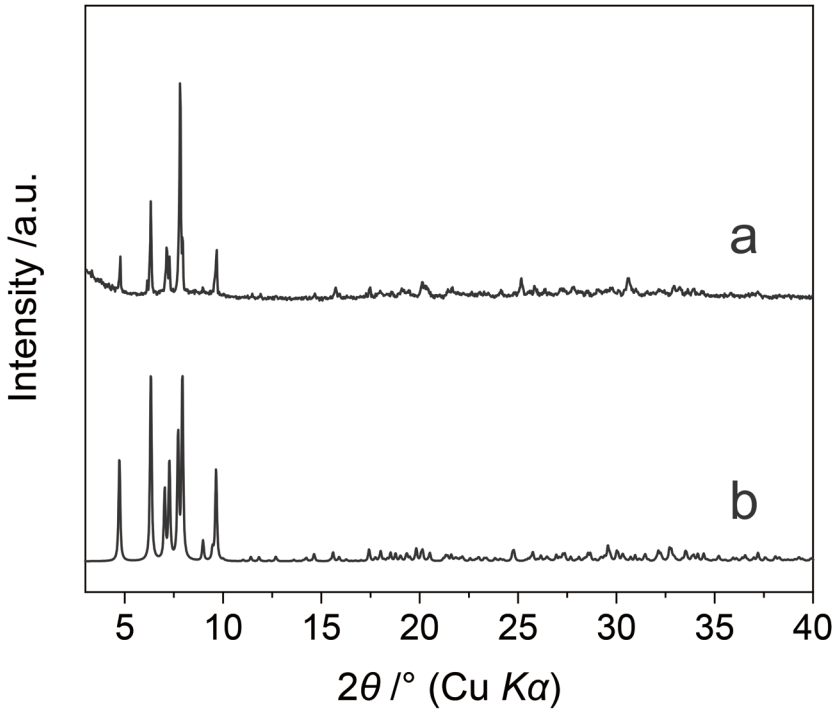

Fig. S1 PXRD patterns of **δ-Al$_{13}$-CoW$_{12}$**. (a) Experimental and (b) simulated from the CIF file[9].

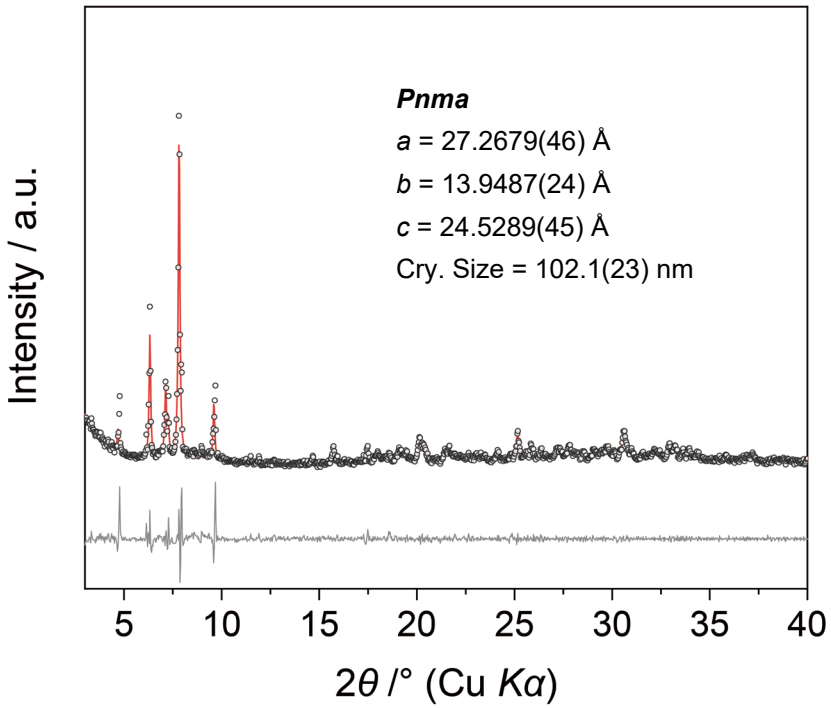

Fig. S2 Experimental (open circles) and calculated (red solid line) PXRD patterns of **δ-Al$_{13}$-CoW$_{12}$** by the Le Bail method. The bottom line shows the difference profile.

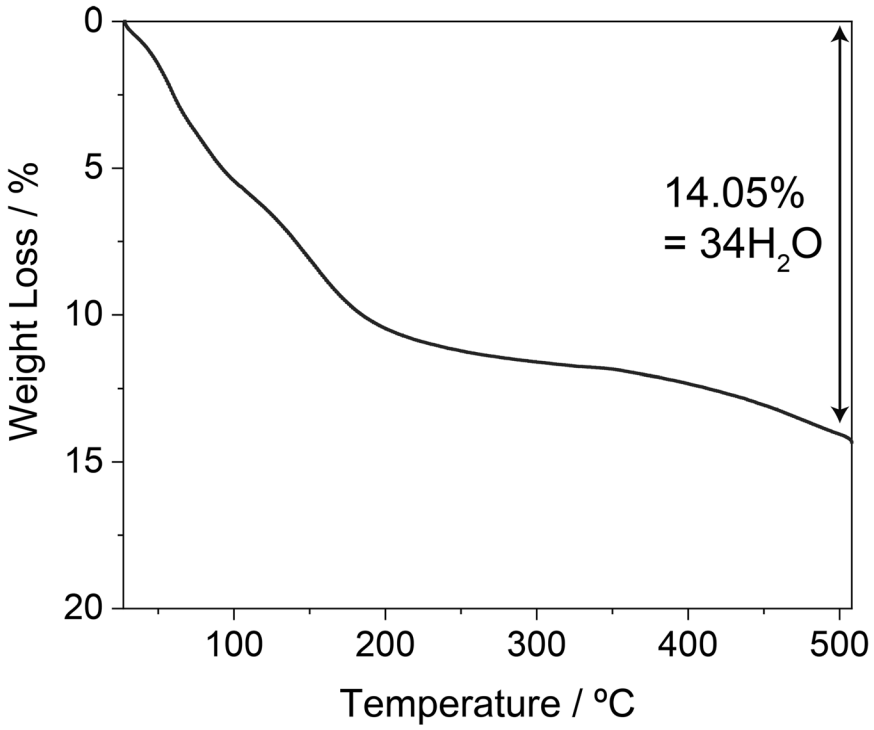

Fig. S3 TGA curves of **δ-Al$_{13}$-CoW$_{12}$**. The weight loss after the measurement was 14.05%. Assuming that the water of crystallization in **δ-Al$_{13}$-CoW$_{12}$** and that the water molecules coordinated to **δ-Al$_{13}$** ($12H_2O$) are lost after the measurement, the amount of water of crystallization in **δ-Al$_{13}$-CoW$_{12}$** was determined as $22H_2O$.

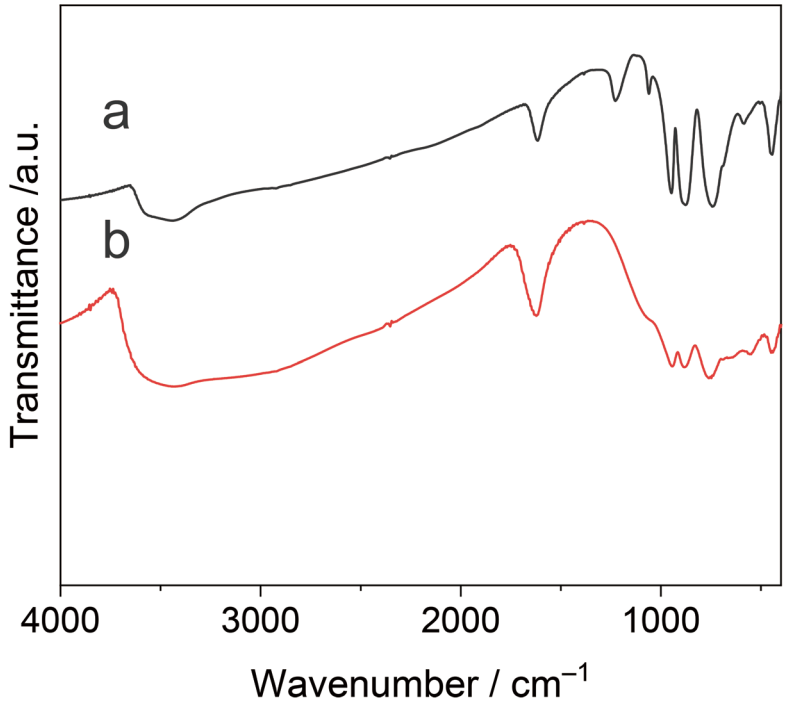

Fig. S4 IR spectra of (a) **δ-Al$_{13}$-CoW$_{12}$** and (b) $K_6[\alpha\text{-}CoW_{12}O_{40}]\cdot nH_2O$. KBr pellet ($cm^{-1}$): 943 ν(W=O), 883 ν(W−O_c−W), 760 ν(W−O_e−W, Al−O_{Td}), 642 ν(Al−OH_{Oh}), 550 ν(Al−OH_{Oh}), 441 ν(Al−OH_{2Oh}).

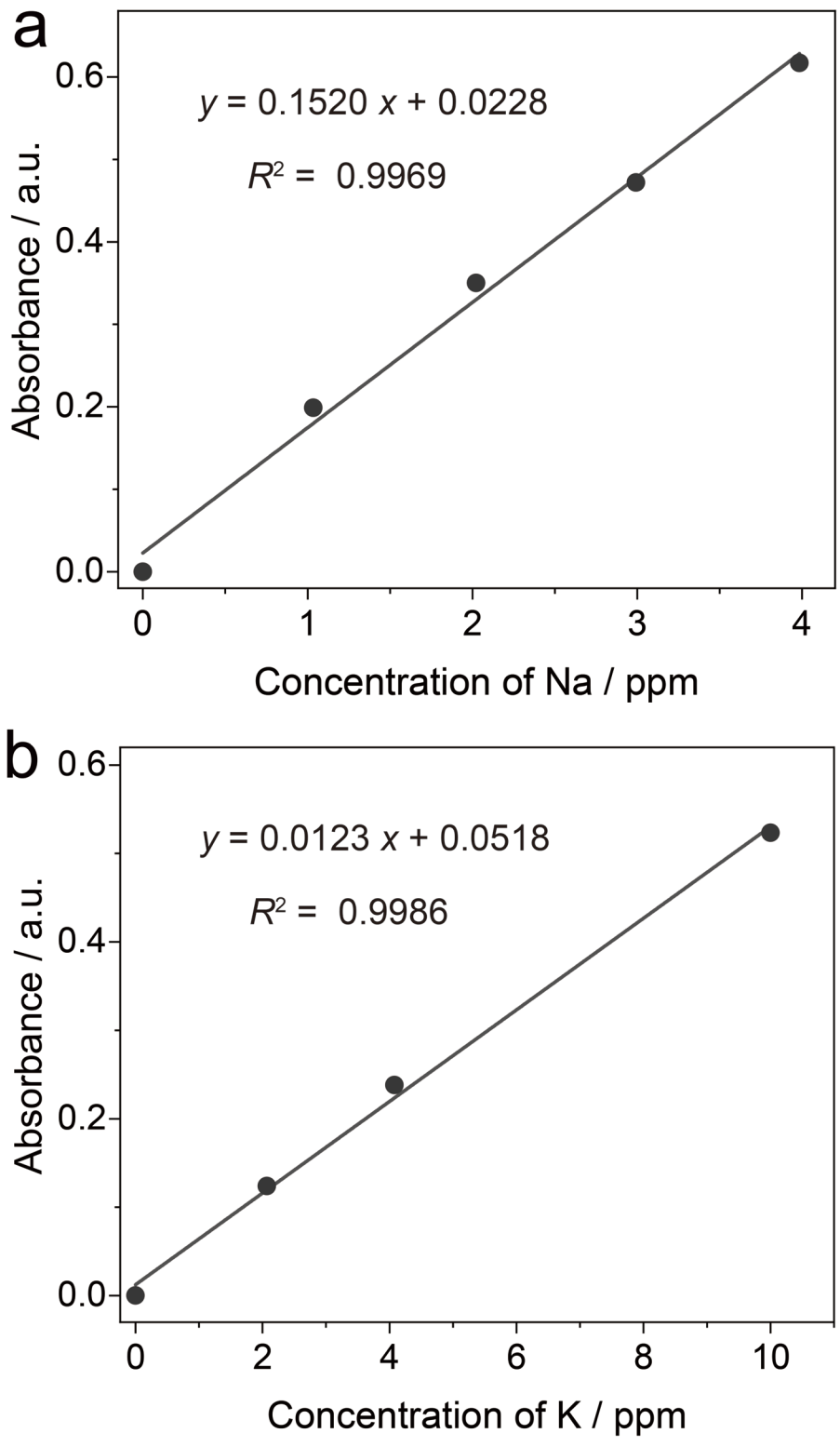

Fig. S5 Calibration curves of (a) Na (λ = 589.0 nm) and (b) K (λ = 766.5 nm) in AAS. Absorbance values of the sample solution at λ = 589.0 nm and 766.5 nm were 0.0155 and 0.0034, respectively, and were negligible. If one Na^+ or K^+ instead of proton (H^+) were contained in **δ-Al$_{13}$-CoW$_{12}$**, the concentration of Na or K would be ca. 0.5 ppm and detectable. These results show that **δ-Al$_{13}$-CoW$_{12}$** does not contain these elements.

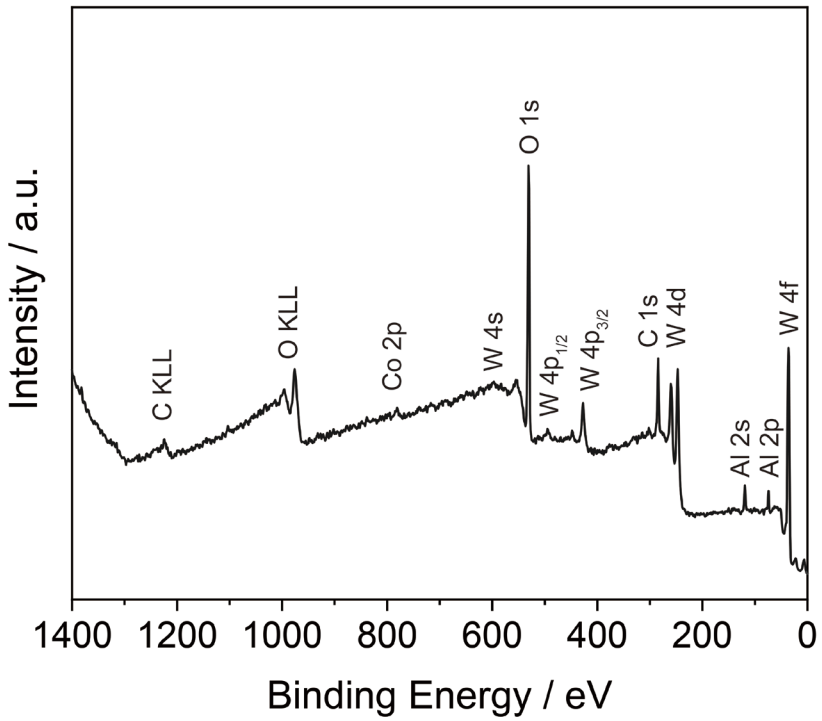

Fig. S6 Wide scan XPS spectrum of **δ-Al$_{13}$-CoW$_{12}$**. Note that the Cl 2p signal (around 200 eV) was absent, suggesting that Cl^- does not exist to compensate the surplus cation charge. In addition, ion-exchange chromatography measurement showed that Cl is below the detection limit.

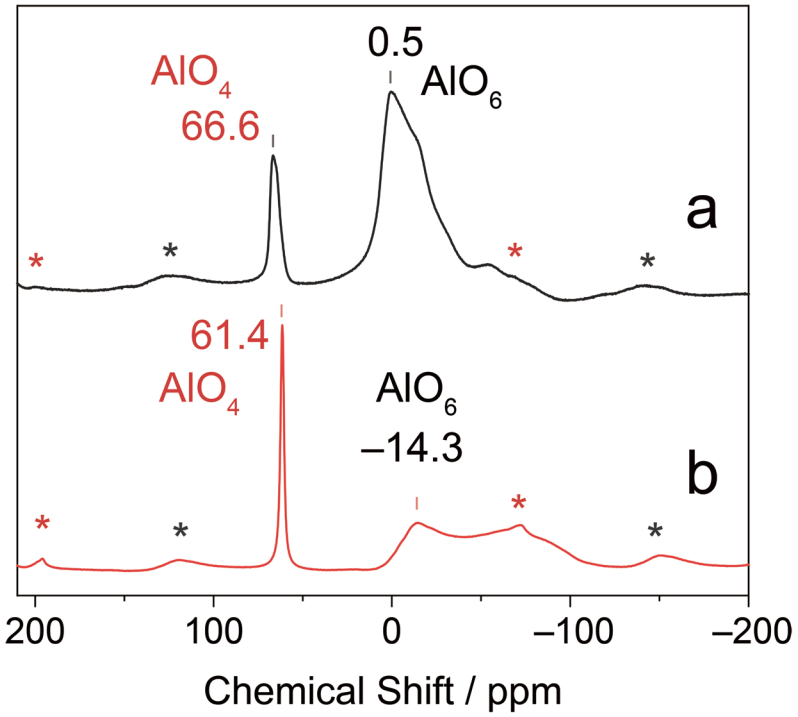

Fig. S7 Solid-state ^{27}Al-MASNMR spectra of (a) **δ-Al$_{13}$-CoW$_{12}$** and (b) **ε-Al$_{13}$-CoW$_{12}$**. Black and red asterisks indicate the spinning side bands (MAS rate = 14 kHz) originating from the signals of AlO_6 and AlO_4 sites, respectively.

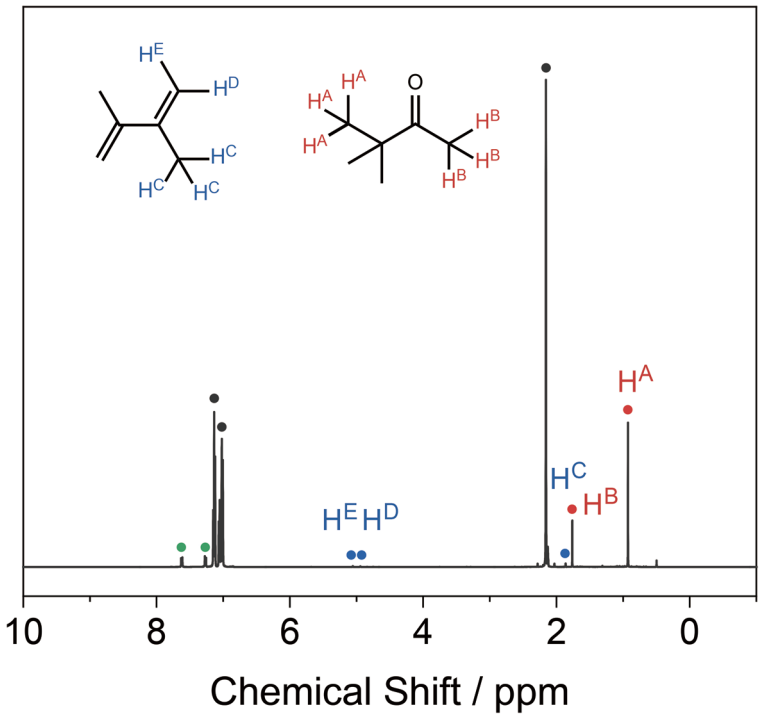

Fig. S8 Solution ^{1}H-NMR spectrum (toluene-d_8) of the filtrate after the pinacol rearrangement catalyzed by **δ-Al$_{13}$-CoW$_{12}$**. The signals labelled by red, blue, green, and black circles correspond to pinacolone, 2,3-dimethyl-1,3-butadiene, naphthalene, and toluene, respectively. Reaction conditions: pinacol (0.667 mmol), naphthalene (0.267 mmol), and catalyst (0.067 mmol) in 2 mL toluene at 373 K for 10 h.

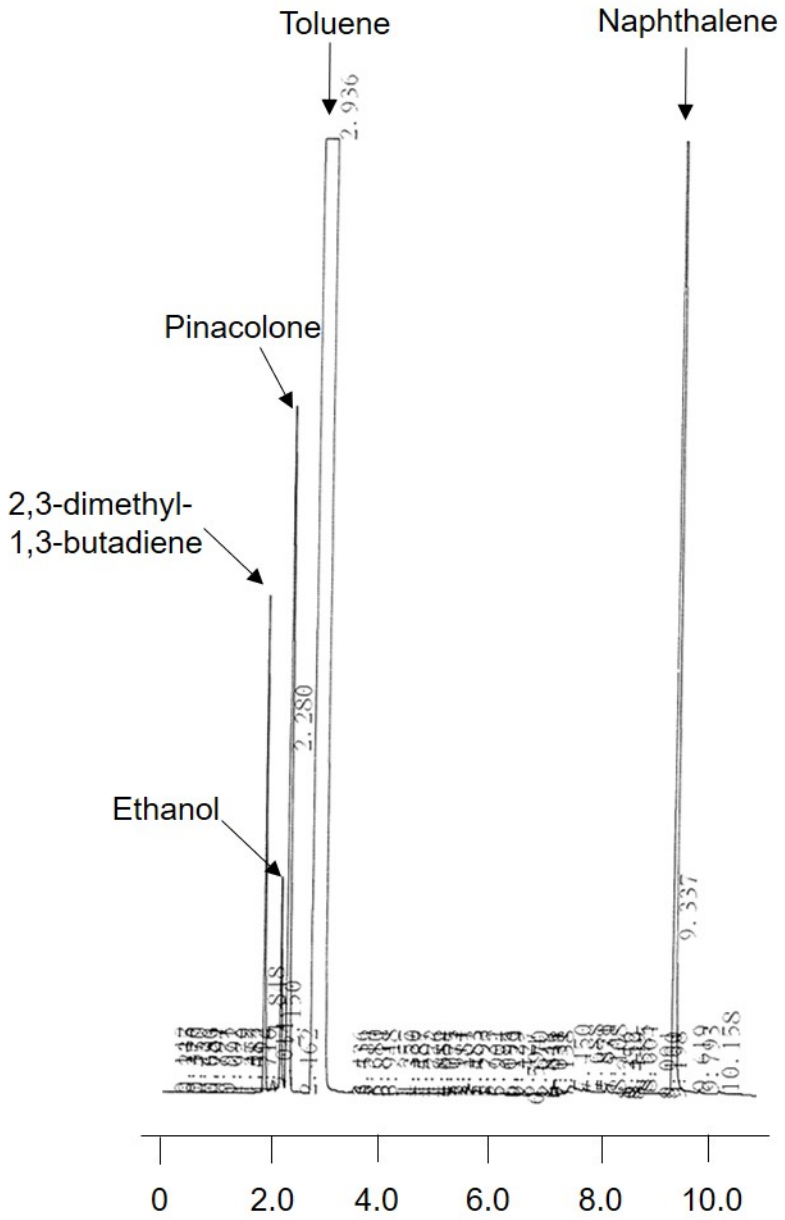

Fig. S9 GC chart of the pinacol rearrangement catalyzed by **δ-Al$_{13}$-CoW$_{12}$**. The retention times of 2,3-dimethyl-1,3-butadiene, pinacolone, toluene, pinacol, and naphthalene are 1.8, 2.3, 2.9, 7.3, and 9.3 min, respectively. Reaction conditions: pinacol (0.667 mmol), naphthalene (0.267 mmol), and catalyst (0.067 mmol) in 2 mL toluene at 373 K for 10 h. Ethanol is used as a washing solvent.

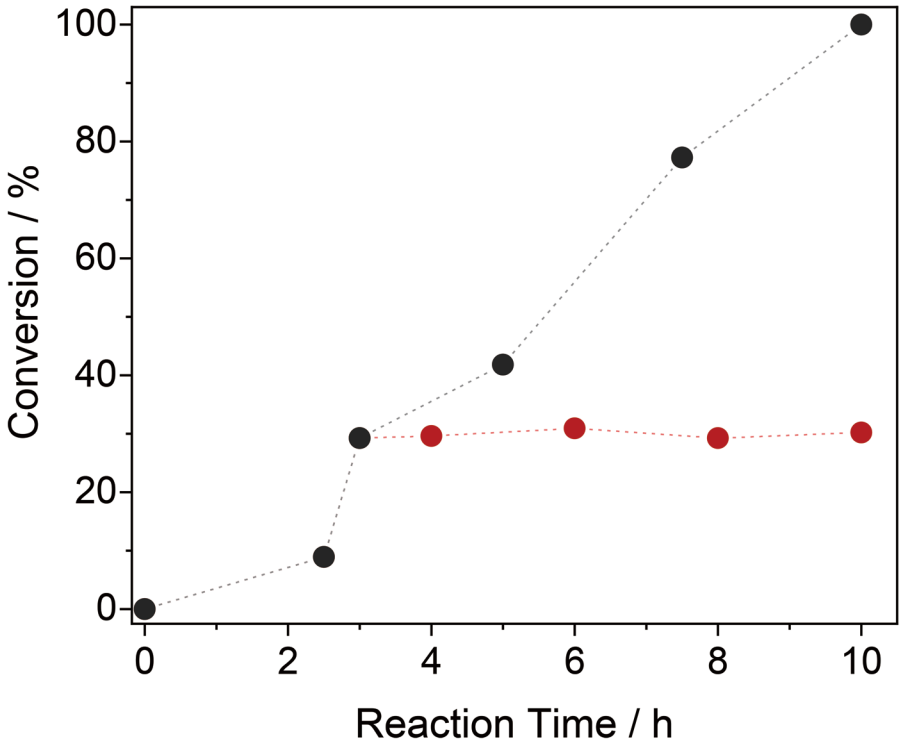

Fig. S10 Time courses of pinacol rearrangement catalyzed by **δ-Al$_{13}$-CoW$_{12}$** at 373 K (black) and after removal of the catalyst (red).

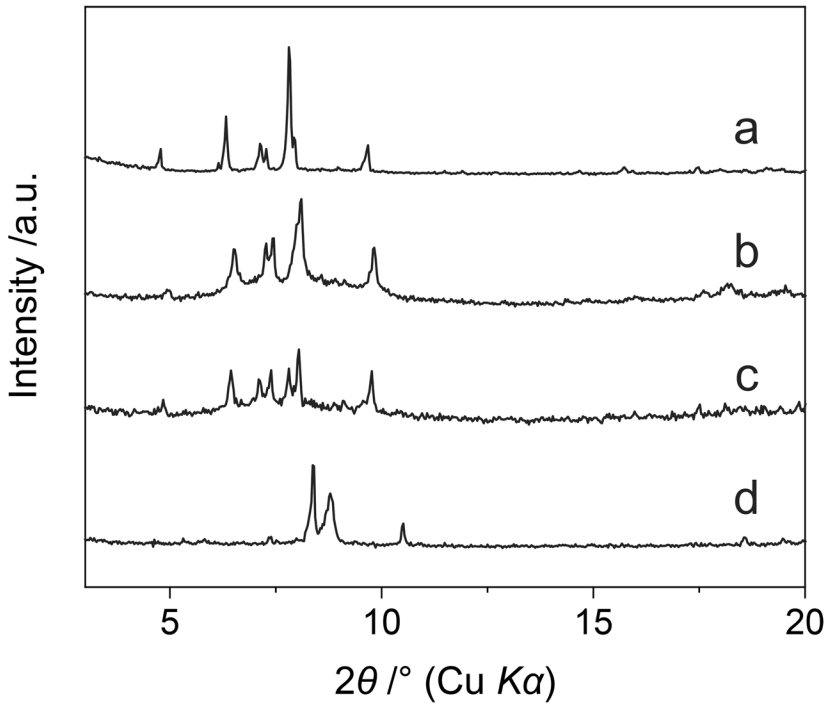

Fig. S11 PXRD patterns of **δ-Al$_{13}$-CoW$_{12}$**. (a) As synthesized, (b) after reaction, (c) after reuse, and (d) dried at 373 K for 24 h.

References

1 K. Mizuno, T. Mura, and S. Uchida, *Cryst. Growth Des.*, 2016, **16**, 4968−4974.

2 L. C. W. Baker and V. E. Simmons, *J. Am. Chem. Soc*., 1959, **81**, 4744–4745.

3 P. J. Domaille, *J. Am. Chem. Soc*., 1984, **106**, 7677−7687.

4 M. J. Frisch, G. W. Trucks, H. B. Schlegel, G. E. Scuseria, M. A. Robb, J. R. Cheeseman, G. Scalmani, V. Barone, B. Mennucci, G. A. Petersson, H. Nakatsuji, M. Caricato, X. Li, H. P. Hratchian, A. F. Izmaylov, J. Bloino, G. Zheng, J. L. Sonnenberg, M. Hada, M. Ehara, K. Toyota, R. Fukuda, J. Hasegawa, M. Ishida, T. Nakajima, Y. Honda, O. Kitao, H. Nakai, T. Vreven, J. A. Jr. Montgomery, J. E. Peralta, F. Ogliaro,M. Bearpark, J. J. Heyd, E. Brothers, K. N. Kudin, V. N. Staroverov, T. Keith, R. Kobayashi, J. Normand, K. Raghavachari, A. Rendell, J. C. Burant, S. S. Iyengar, J. Tomasi, M. Cossi, N. Rega, J. M. Millam, M. Klene, J. E. Knox, J. B. Cross, V. Bakken, C. Adamo, J. Jaramillo, R. Gomperts, R. E. Stratmann, O. Yazyev, A. J. Austin, R. Cammi, C. Pomelli, J. W. Ochterski, R. L. Martin, K. Morokuma, V. G. Zakrzewski, G. A. Voth, P. Salvador, J. J. Dannenberg, S. Dapprich, A. D. Daniels, O. Farkas, J. B. Foresman, J. V. Ortiz, J. Cioslowski and D. J. Fox,Gaussian 09, Rev. D.01; Gaussian, Inc.: Wallingford, CT, 2013.

5 (a) A. D. Becke, *J. Chem. Phys.* 1993, **98**, 5648–5652. (b) C. Lee, C. Yang and R. G. Parr, *Phys. Rev. B*, 1988, **38**, 785–789.

6 P. J. Hay and W. R. Wadt, *J. Chem. Phys.*, 1985, **82**, 299–310.

7 (a) M. M. Francl, W. J. Pietro, W. J. Hehre, J. S. Binkley, M. S. Gordon, D. J. Defrees and J. A. Pople, *J. Chem. Phys.*, 1982, **77**, 3654–3665. (b) P. C. Hariharan and J. A. Pople, *Theor. Chem. Acc.*, 1973, **28**, 213–222. (c) G. A. Petersson, T. G. Tensfeldt and J. A. Montgomery, *J. Chem. Phys.*, 1991, **94**, 6091–6101.

8 J. Tomasi, B. Mennucci and R. Cammi, *Chem. Rev.*, 2005, **105**, 2999–3093.

9 J. H. Son, Y.-U. Kwon and O. H. Han, *Inorg. Chem*., 2003, **42**, 4153–4159.